Sulfonate Ligands-Induced Formation of Alkali Metal - Cucurbit[5]uril-based Assemblies

Jing Xu[a], Qing Wang[a], Wei-Wei Ge[a], Dong Wu*[b], Carl Redshaw[c], Kai Chen*[a]

[a] *Collaborative Innovation Center of Atmospheric Environment and Equipment Technology; Jiangsu Key Laboratory of Atmospheric Environment Monitoring and Pollution Control; Nanjing University of Information Science & Technology, Nanjing 210044, P. R. China. Email: catqchen@163.com*

[b] *Computer Aided Drug Discovery Center, Zhuhai Institute of Advanced Technology, Chinese Academy of Sciences, Zhuhai 519003, China. wudong@ziat.ac.cn*

[c] *Department of Chemistry, School of Natural Sciences, University of Hull, Hull HU6 7RX, UK.*

Abstract: Herein, we report the use of 1,5-naphthalene disulfonic acid (H_2NDS) as a structure-directing agent to construct cucurbit[5]uril-based supramolecular assemblies. In order to demonstrate the directing role played by H_2NDS, {Q[5]·3[H_3O]·3Cl·4H_2O} (**1**) and {Q[5]·H_2NDS·12H_2O} (**2**) were separately synthesized by recrystallization of Q[5] from the HCl solution in both the absence and in the presence of H_2NDS. Following the addition of alkali metal cations to the Q[5]-H_2NDS system, four novel assemblies with the formulae {[$Na_2(H_2O)_2$(Q[5])$(NDS)_{0.5}$]·$(NDS)_{0.5}$} (**3**), {[$K_2(H_2O)_3$(Q[5])]·(NDS)} (**4**), {[$Rb_2(H_2O)_4$(Q[5])]·(NDS)} (**5**) and {[$Cs_2(H_2O)_5$(Q[5])]·(NDS)} (**6**) were obtained. Single-crystal X-ray diffraction studies revealed that all of these metal-containing assemblies have a similar general structure to that of **2**, with the main differences being the coordination modes of the metal cations in **3**-**6**. Furthermore, dye adsorption experiments revealed that compound **2** is able to capture acridine red (AR), indigo carmine (IC), crystal violet (CV) and methylene blue (MB) from aqueous media and the resulting dye-loaded samples can function as solid fluorescence materials.

Introduction

Dyes are a relatively large group of colored organic molecules with complicated structures that can stain other substances and have been extensively used in various industrial applications, such as for the production of food, textiles, plastics, paper, leather, rubber, pharmaceuticals and so on. [1-3] The direct discharge of wastewater containing dyes is, without any treatment, quite harmful to the environment. Moreover, due to toxic effects combined with high solubility in aqueous media and difficulties associated with degradation, dyes can enter the food chain via aquatic life and thus there is also a significant threat to human health. [4,5] Previous studies have documented that numerous dyes are hazardous and can cause damage to the central nervous system, reproductive system, kidney, brain and liver of the human body and can result in even more terrible effects including carcinogenic, teratogenic, mutagenic. [6-9] Therefore, there is an urgent need to remove dyes from wastewater, particularly since this has become one of the main global environment issues. Among the existing developed treatment methods for dye wastewater, the use of adsorption is the most promising and is widely used in the immobilization of dyes from wastewater due to its low cost, high efficiency and easy operation. [10] To-date, a variety of materials have been explored for their adsorption capability toward dyes, such as zeolites, clays, polymers, hydrogels, nanocomposites, metal-organic frameworks (MOFs), metal-organic cages, covalent organic frameworks (COFs) and so on. [11-18]

Recent decades have witnessed a boom in the development of supramolecular architectures and materials constructed from different non-covalent interactions, such as π…π stacking, C-H…π interactions, hydrogen bonding, hydrophobic interactions, electrostatic interactions etc. This has been driven by their fascinating structures and promising applications in the likes of molecular adsorption/separation, sensing, catalysis, biomaterials and so on. [19-23] Meanwhile, they also find a role in wastewater treatment including dye removal. [24-26] As a relatively new generation of macrocyclic molecules, cucurbit[*n*]urils (Q[*n*]s, n = 5-8, 10, 14, 15) are pumpkin-shaped macrocycles composed of *n* glycoluril units linked by 2*n* methylene groups. [27] The distinguishing features of their structure is that they possess a hydrophobic cavity and two polar portals lined with carbonyl groups, and these features have aroused the

interest of both the supramolecular and coordination chemistry communities since Q[6] was first structurally determined by Mock and coworkers in 1981. [28-33] The hydrophobic cavity of the Q[*n*]s can accommodate specific guest molecules to form host-guest complexes and the polar portals are capable of coordinating with different metal ions to afford coordination complexes. [34, 35] In recent years, it has also determined that the electropositive outer surface of the Q[*n*]s can be involved in various non-covalent interactions to build supramolecular materials. [36-41] Therefore, the Q[*n*] family has become one of the most attractive molecules in the field of supramolecular chemistry. With the advancement of studies on Q[*n*]s, the adsorption capacity of Q[*n*]-based materials for the removal of dyes have also been investigated, especially for porous self-assemblies based on the outer-surface of Q[*n*]s. For example, Tao and coworkers reported a Q[10]-$[Cd_4Cl_{16}]^{8-}$-based pillared diamond supramolecular framework that could absorb guest dyes, such as rhodamine B, pyrenemethanamine hydrochloride and bathocuproine hydrochloride, and further generated solid materials with efficient red-green-blue fluorescence. [36]

Herein, we introduced 1,5-naphthalene disulfonic acid (H_2NDS) as a structure-directing agent and react it with Q[5] and alkali metal ions to build supramolecular self-assemblies. Firstly, in order to demonstrate the directing role of H_2NDS, Q[5]-based and Q[5]-NDS^{2-}-based supramolecular assemblies with the formula of $\{Q[5]\cdot 3[H_3O]\cdot 3Cl\cdot 4H_2O\}$ (**1**) and $\{Q[5]\cdot H_2NDS\cdot 12H_2O\}$ (**2**) were obtained by the recrystallization of Q[5] from HCl solution in both the absence and presence of H_2NDS respectively. Then, by the introduction of M_{alkali}^{+} cations into the Q[5]-H_2NDS system, four novel assemblies $\{[Na_2(H_2O)_2(Q[5])(NDS)_{0.5}]\cdot(NDS)_{0.5}\}$ (**3**), $\{[K_2(H_2O)_3(Q[5])]\cdot(NDS)\}$ (**4**), $\{[Rb_2(H_2O)_4(Q[5])]\cdot(NDS)\}$ (**5**) and $\{[Cs_2(H_2O)_5(Q[5])]\cdot(NDS)\}$ (**6**) were synthesized. Single-crystal X-ray diffraction (SC-XRD) analysis revealed that compounds **3**-**6** possess a similar general structure to that of **2** with the main difference being the coordination modes of the M_{alkali}^{+} cations. Furthermore, dye adsorption experiments were carried out to explore the removal capacity of compound **2** for dyes. The results revealed that **2** could effectively absorb acridine red (AR), indigo carmine (IC), crystal violet (CV) and methylene blue (MB)

and the dye-loaded samples could function as solid fluorescence materials.

Experimental section

Materials and methods.

All reagents and solvents were commercially purchased and used as received without further purification. Q[5] was synthesized according to the previous literature methods. [42] Elemental analyses for C, H and N were performed on a Perkin-Elmer 240C Elemental Analyzer. FT-IR spectra were recorded in the range of 400-4000 cm^{-1} on a Bruker Vector 22 FT-IR spectrophotometer using KBr pellets. Thermogravimetric analyses (TGA) were conducted on a Mettler-Toledo (TGA/DSC1) thermal analyzer under nitrogen with a heating rate of 10 °C·min^{-1}. Powder X-ray diffraction (PXRD) data for all samples were collected at room temperature on bulk samples with Cu Kα radiation (1.54059 Å) on a Bruker D8 Advance X-ray diffractometer, in which the X-ray tube was operated at 40 kV and 40 mA. UV-vis measurements were carried out at room temperature on a Shimadzu UV3600 spectrophotometer.

Preparation of {Q[5]·3[H_3O]·3Cl·4H_2O} (1). The powder samples of Q[5] (8.5 mg, 0.008 mmol) were dissolved in HCl solution (0.1 M, 5 mL) and then left to stand at room temperature. After 3 days, colorless crystals of **1** were obtained in 75% yield.

Preparation of {Q[5]·H_2NDS·12H_2O} (2). A mixture of Q[5] (8.5 mg, 0.008 mmol) of 1,5-H_2NDS (10.48 mg, 0.008 mmol) was dissolved in 9 mL deionized water with stirring at room temperature. The solution was sealed in a Teflon-lined stainless-steel vessel and then heated at 100 ℃ for 8 h. After cooling to room temperature, orange crystals of **2** were collected in 36% yield.

Preparation of {[Na_2(H_2O)$_2$(Q[5])(NDS)$_{0.5}$]·(NDS)$_{0.5}$} (3). A mixture of Q[5]·10H_2O (8.5 mg, 0.008mmol) and NaCl (2.8 mg, 0.048 mmol) in deionized water (10 mL) was stirred at room temperature for 1 h and then 1,5-H_2NDS (5.76 mg, 0.025 mmol) was added. The resulting mixture was sealed in a Teflon-lined stainless-steel vessel and then heated at 100 °C for 8 h. After cooling to room temperature, light yellow block crystals of **3** were obtained in 32 % yield based on Q[5]·10H_2O.

Preparation of {[K_2(H_2O)$_3$(Q[5])]·(NDS)} (4). Compound **4** was prepared by the

same procedure used for preparation of **3** except that NaCl was used instead of KCl (3.55 mg, 0.048 mmol). Yellow block crystals of **4** were obtained in 39 % yield based on Q[5]·10H_2O.

Preparation of {[$Rb_2(H_2O)_4$(Q[5])]·(NDS)} (5). Compound **5** was prepared by the same procedure used for preparation of **3** except that NaCl was used instead of RbCl (5.80 mg, 0.048 mmol). Yellow block crystals of **5** were obtained in 39 % yield based on Q[5]·10H_2O.

Preparation of {[$Cs_2(H_2O)_5$(Q[5])]·(NDS)} (6). Compound **6** was prepared by the same procedure used for preparation of **3** except that NaCl was used instead of CsCl (8.08 mg, 0.048 mmol). Yellow block crystals of **6** were obtained in 39 % yield based on Q[5]·10H_2O.

Adsorption experiments

In this study, batch adsorption experiments were performed using the following method: 50 mg adsorbent was mixed with 50 mL dye aqueous solution with a certain concentration in a 150 mL closed conical flask. Stock solutions of the five dyes including acridine red (**AR**), indigo carmine (**IC**), crystal violet (**CV**), methyl orange (**MO**) and methylene blue (**MB**) were prepared in deionized water (0.05 mM). The desired experimental solutions of dyes were obtained by successive dilution of these stock solutions with deionized water. The adsorption of AR, IC, CV, MO and MB on compounds **2** was studied at different adsorption times (30-150 min) at room temperature. All the experiments were performed at a constant stirring rate of 300 rpm. After stirring for a certain time, the adsorbent was removed by centrifugation before the measurements, and the corresponding supernatant was analyzed by UV-vis spectra at 527 nm for AR, 286 nm for IC, 575 nm for CV, 464 nm for MO and 664 for MB. The calibration curves of the dyes were first obtained and used to convert absorbance data into concentrations during the adsorption experiments.

X-ray crystallography

Crystallographic data collections for **1**-**6** were carried out on a Bruker Smart Apex II CCD area-detector diffractometer with graphite-monochromated Mo Kα radiation (λ = 0.71073 Å) using ω-scan technique. The diffraction data were integrated by using the

SAINT program, [43] which was also used for the intensity corrections for the Lorentz and polarization effects. Semi-empirical absorption correction was applied using the *SADABS* program. [44] The structures were solved by direct methods and all the non-hydrogen atoms were refined anisotropically on F^2 by the full-matrix least-squares technique using the SHELXL-2018 crystallographic software package. [45] All non-hydrogen atoms were refined anisotropically and hydrogen atoms were introduced at the calculated positions. The details of the crystal parameters, data collection and refinements for the complexes are summarized in the Table 1, and selected bond lengths and angles with their estimated standard deviations are listed in **Table S1**.

Table 1. Crystal Data and Structure Refinements for **1**-**6**.

Compound	**1**	**2**	**3**	**4**	**5**	**6**
chemical formula	$C_{30}H_{30}N_{20}O_{17}Cl_3$	$C_{40}H_{36}N_{20}O_{28}S_2$	$C_{40}H_{36}N_{20}O_{18}S_2Na_2$	$C_{40}H_{36}N_{20}O_{19}S_2K_2$	$C_{40}H_{36}N_{20}O_{19}S_2Rb_2$	$C_{40}H_{36}N_{20}O_{19}S_2Cs_2$
formula weight	1049.09	1309.01	1194.99	1243.21	1351.95	1243.21
crystal system	Monoclinic	Monoclinic	Monoclinic	Monoclinic	Monoclinic	Monoclinic
space group	C_2/m	P_{21}/c	P_{21}/c	P_{21}/c	P_{21}/c	P_{21}/c
a /Å	25.082(2)	12.7096(3)	12.469(5)	12.274(5)	12.449(5)	12.681(5)
b /Å	14.4962(14)	15.9515(4)	15.956(5)	16.173(5)	16.143(5)	16.214(5)
c /Å	14.7769(14)	27.0718(7)	27.061(5)	27.018(5)	26.916(5)	27.109(5)
β /°	101.766(2)	96.4100(10)	95.919(5)	94.661(5)	95.226(5)	96.033(5)
temperature /K	293(2)	193(2)	293(2)	293(2)	293(2)	173(2)
volume /Å^3	5259.9(8)	5454.1(2)	5355(3)	5346(3)	5525.5(13)	5543(3)
Z	4	4	4	4	4	4
D_c /g cm^{-3}	1.325	1.594	1.482	1.545	1.643	1.727
μ /mm^{-1}	0.254	1.211	0.206	0.348	1.598	6.704
F(000)	2148	2688	2456	2552	964	5005
reflections collected /unique	4827 / 3717	9614 / 7394	9412 / 5339	9399 / 6845	9460 / 7174	9695 / 6974
data / restraints / parameters	4827 /0 /330	9614 / 0 / 811	9412 /0 /734	9399 / 0 /752	9460 / 0 / 757	9695 / 0 /802
GOF	1.022	1.174	0.1076	1.119	1.009	1.011
R_1, wR_2 [$I > 2\sigma(I)$][a,b]	R_1=0.0703, wR_2=0.1577	R_1=0.0539, wR_2=0.1587	R_1=0.0644, wR_2=0.1672	R_1=0.0658, wR_2=0.1470	R_1=0.0628, wR_2=0.1270	R_1=0.0648, wR_2=0.1570
R_1, wR_2 (all data)	R_1=0.0830, wR_2=0.1622	R_1=0.0711, wR_2=0.1696	R_1=0.973, wR_2=0.1875	R_1=0.0837, wR_2=0.1536	R_1=0.0855 wR_2=0.1436	R_1=0.0925 wR_2=0.1656

[a] $R_1 = \Sigma||F_o| - |F_c||/\Sigma|F_o|$. [b] $wR_2 = |\Sigma w(|F_o|^2 - |F_c|^2)|/\Sigma|w(F_o)^2|^{1/2}$, where $w = 1/[\sigma^2(F_o^2) + (aP)^2 + bP]$. $P = (F_o^2 + 2F_c^2)/3$

RESULTS AND DISCUSSION

Crystal Structure of {Q[5]·3[H_3O]·3Cl·4H_2O} (1). According to the SC-XRD analysis, compound **1**, which was recrystallized by dissolving Q[5] in the HCl solution, belonged to the monoclinic *C*2/*m* space group. As depicted in Figures 1a and 1b, the adjacent Q[5] molecules generate a one-dimensional (1D) supramolecular chain via the hydrogen bonds among the carbonyl groups of Q[5], the free H_3O^+ ions, water molecules and Cl^- anions. A final 3D supramolecular framework was constructed from these 1D chains via the hydrogen bonds between the methylene/methyne groups at the outer surface of Q[5] and the free water molecules and Cl^- anions (**Figs. 1c-1e**). Furthermore, hexagonal channels along the *c*-axis were observed and these channels are filled by free water molecules and Cl^- anions (**Fig. 1e**).

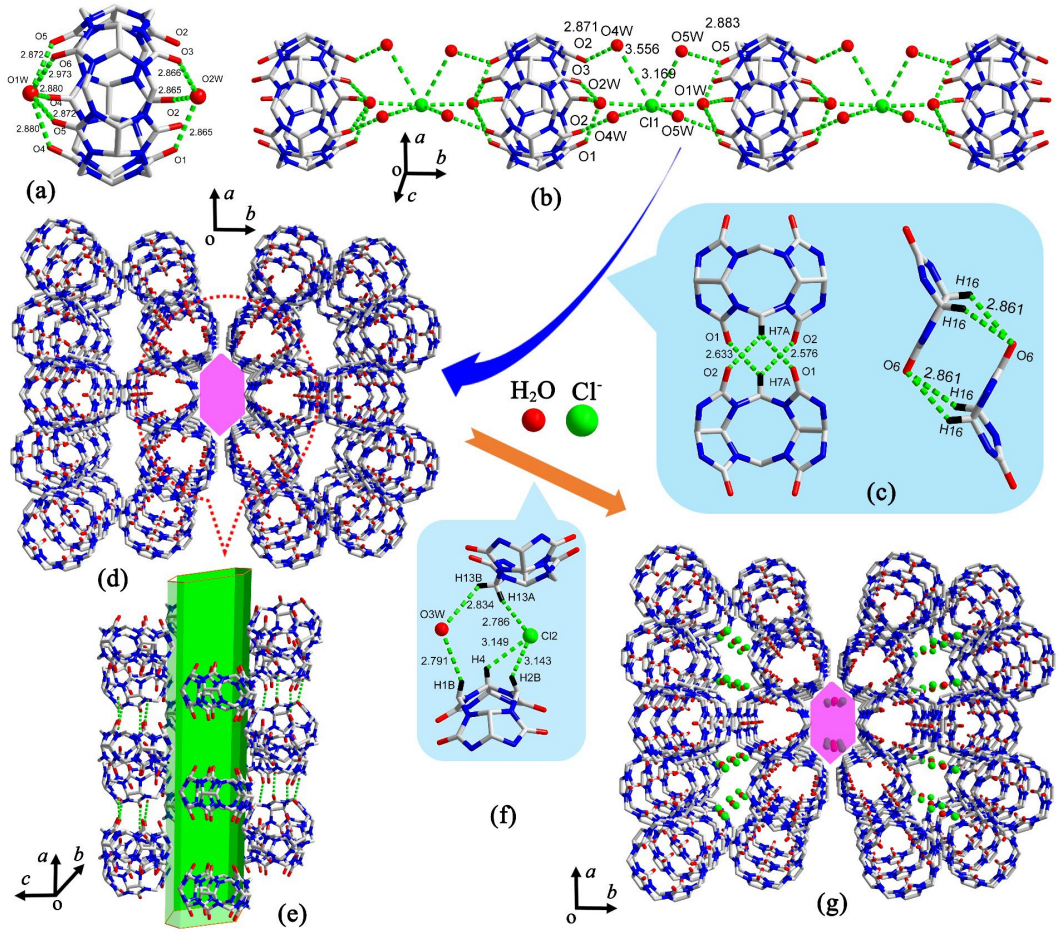

Figure 1. (a, b) Hydrogen bonding among the carbonyl groups of Q[5], free H_3O^+, water molecules and Cl^- anions; (c) The Q[5]-based 3D supramolecular framework with 1D hexagonal channel along the *c*-axis; (d) Hydrogen bonding between the methylene/methyne groups at the outer surface of Q[5] and free water molecules and Cl^- anions; (e) The final 3D architecture of **1**.

Crystal Structure of {Q[5]·H_2NDS·12H_2O} (2). The SC-XRD analysis revealed that assembly **2** crystallized in the monoclinic $P2_1/c$ space group and each asymmetric unit contains one Q[5] molecule and two crystallographically independent half 1,5-NDS^{2-} anions. As depicted in Figure 2a, the Q[5]s interact with each other *via* hydrogen bonds between the carbonyl groups and the free water molecules to give 1D supramolecular chains and these chains further generate a Q[5]-based supramolecular framework via π…π interactions between the carbonyl groups and the hydrogen bonds between the carbonyl groups and the methylene/methyne groups at the outer surface of the Q[5] (**Figs. 2b** and **2c**). Furthermore, it is worth noting that there are 1D hexagonal channels along the *a*-axis (**Fig. 2g**). As for the sulfonate ligands, the 1,5-NAS^{2-} anions join together to generate 1D supramolecular chains via C-H…π and hydrogen bonding interactions and these chains are trapped in the hexagonal channels through various noncovalent interactions between the outer surface of the Q[5] and sulfonate ligands, such as the π…π, C-H…π and hydrogen bonding interactions (**Figs. 2d** and **2e**).

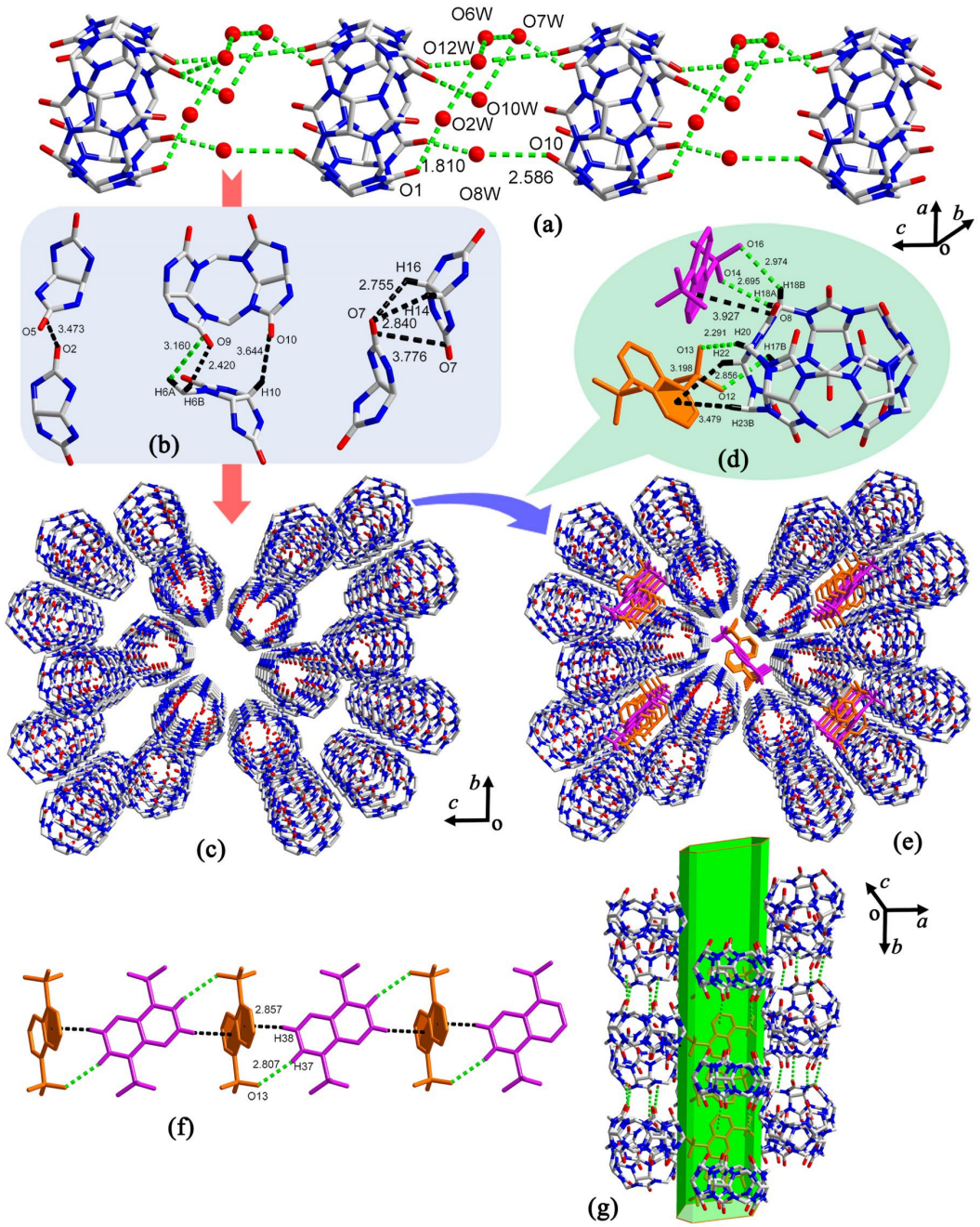

Figure 2. (a) Structure representation of the components of **2** and the 1D supramolecular chain constructed from the hydrogen bonds between the Q[5] and free water molecules; (b) Interactions between adjacent Q[5] molecules; (c) The 3D supramolecular framework constructed from the Q[5]-based chains; (d) The interactions between the outer surface of Q[5] and 1,5-NAS^{2-}; (e) Final 3D structure of **2**; (f) Interactions between sulfonate ligands 1,5-NAS^{2-}; (g) Hexagonal channels in **2**.

Crystal Structure of $\{[Na_2(H_2O)_2(Q[5])(NDS)_{0.5}]\cdot(NDS)_{0.5}\}$ (3), $\{[K_2(H_2O)_3(Q[5])]\cdot(NDS)\}$ (4), $\{[Rb_2(H_2O)_4(Q[5])]\cdot(NDS)\}$ (5), $\{[Cs_2(H_2O)_5(Q[5])]\cdot(NDS)\}$ (6). The SC-XRD analysis revealed that the assemblies **3-6** possess a similar structure to that observed for **2**, with the main difference being the

coordination modes of the alkali metal ions. Each asymmetric unit of **3** contains one $\{[Na_2(H_2O)_2(Q[5])(1,5\text{-}NDS^{2-})_{0.5}]\cdot(1,5\text{-}NDS^{2-})_{0.5}\}$ molecule. As shown in Figure 3, Na1 adopted a distorted pentagonal pyramidal coordination geometry and coordinates with six oxygen atoms including five carbonyl oxygen atoms from the same portal of Q[5] (O6, O7, O8, O9, O10) and one coordinated water molecule (O1W), while Na2 is bound to three oxygen atom in a distorted triangular pyramidal geometry including one carbonyl oxygen atom from Q[5] (O8), sulfonate oxygen atom from the ligand 1,5-NDS^{2-} (O15) and one coordinated water molecule (O2W). It can be observed that the coordination between Q[5] and Na1 gave a molecular bowl-shaped coordination complex and the bonding of Na2 to Q[5] and sulfonate ligands 1,5-NAS^{2-} formed simple ternary Q[5]-Na^+-1,5-NDS^{2-} coordination compounds. Furthermore, these ternary coordination compounds interacted with the uncoordinated sulfonate ligands 1,5-NDS^{2-} *via* C-H…π and hydrogen bonding interactions to give 1D supramolecular chains (**Fig. 4**) and then generated a 2D supramolecular layer (**Fig. 5a**) by the use of π…π interactions between the carbonyl groups of neighboring Q[5]s and hydrogen bonding between the methylene groups on the outer surface and the carbonyl groups of Q[5] (Figure 5b). Finally, these 2D layers assembled into a 3D supramolecular architecture (Figures 6a and 6b) *via* noncovalent interactions between Q[5] molecules and those between the sulfonate ligands 1,5-NDS^{2-} and the outer surface of Q[5] (**Figs. 3c** - **3e**).

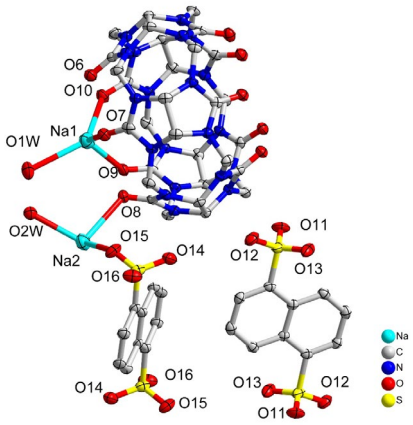

Figure 3. The coordination environment of Na^+ in assembly **3** with displacement ellipsoids drawn at the 50% probability level. Hydrogen atoms was omitted for clarity.

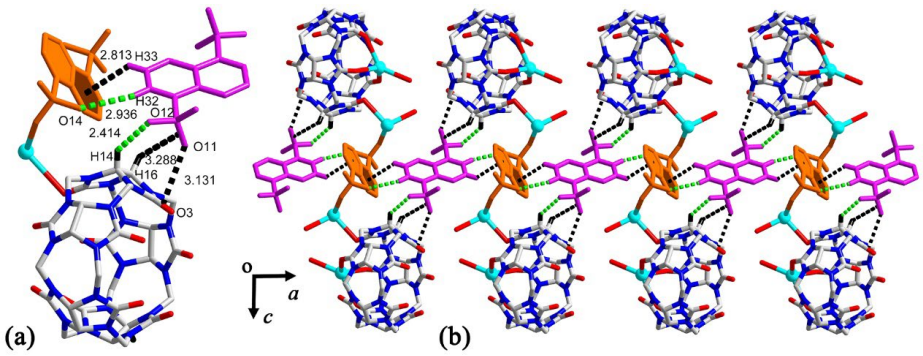

Figure 4. (a) The interaction among the sulfonate ligands 1,5-NAS^{2-} and the outer surface of Q[5] molecules; (b) The ternary Q[5]-Na^{+}-1,5-NAS^{2-} supramolecular chain.

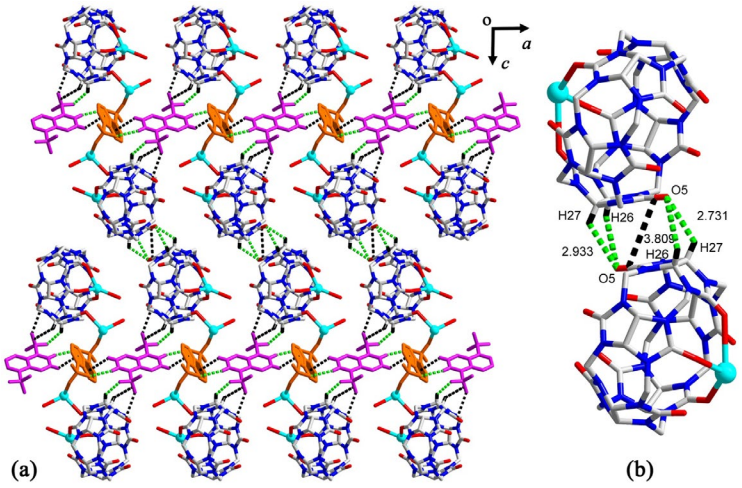

Figure 5. (a) The 2D supramolecular layer (a) constructed from the Q[5]-Na^{+}-1,5-NAS^{2-} chains through the hydrogen bonding interactions between adjacent Q[5] (b).

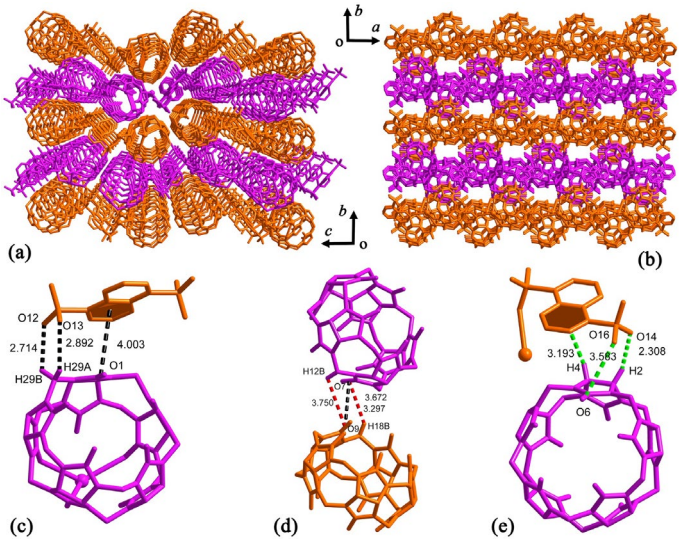

Figure 6. The 3D supramolecular structure of assembly **3** along (a) *a*-axis; (b) and *c*-axis; (c) through the noncovalent interactions between Q[5]s (d) and those between Q[5] and NDS^{2-} (c, e).

According to the SC-XRD analysis, the metal cations in the assemblies **4-6** exhibit

similar coordination modes to Q[5]. In the structures of **4-6**, the portals of the Q[5]s are all covered by alkali metal ions and the distinction mainly lies in the numbers of water molecules bound to central metal ions (Figure 7). The assembly **4** is taken as a representative example to illustrate the structural details. As shown in Figure 8, K1 is coordinated by five carbonyl oxygen atoms from the same portal of Q[5] (O1, O2, O3, O4, O5) and one coordinated water molecule (O1W) in a distorted pentagonal pyramidal coordination geometry, while K2 is bound to five carbonyl oxygen atoms from the same portal of Q[5] (O6, O7, O8, O9, O10) and two coordinated water molecules in a distorted mono-capped triangular prism coordination geometry. Each carbonyl portal of the Q[5] is covered by K^+ cations through coordination to form a capsule-shaped coordination complex, which then forms a 1D supramolecular chain through hydrogen bonds among the coordination waters and the carbonyl groups of Q[5] (Figure 9). These chains can also interact to afford a 3D supramolecular architecture with 1D hexagonal channels filled by sulfonate ligands 1,5-NAS^{2-} (Figure 10). Compounds **5** and **6** also have similar 3D supramolecular architectures to that of **4** (Figure S1).

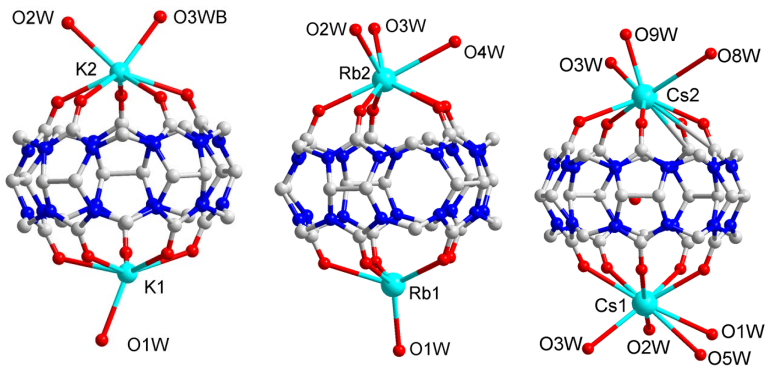

Figure 7. The coordination modes of alkali metal ions with Q[5] molecules in **4-6**.

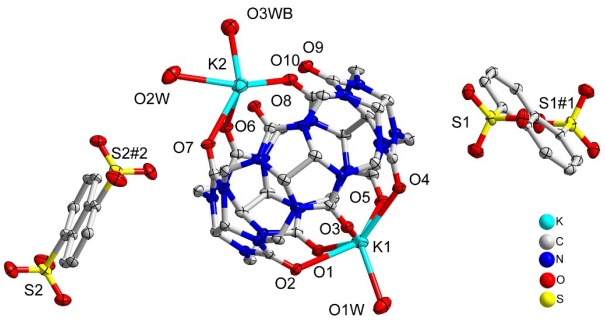

Figure 8. The coordination environment of K^+ in assembly **4** with displacement ellipsoids drawn at the 50% probability level. Hydrogen atoms was omitted for clarity.

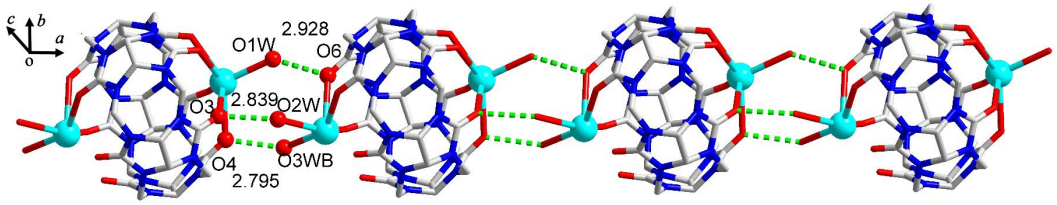

Figure 9. The 1D supramolecular chains constructed via hydrogen bonds among the coordination waters and the carbonyl groups of Q[5].

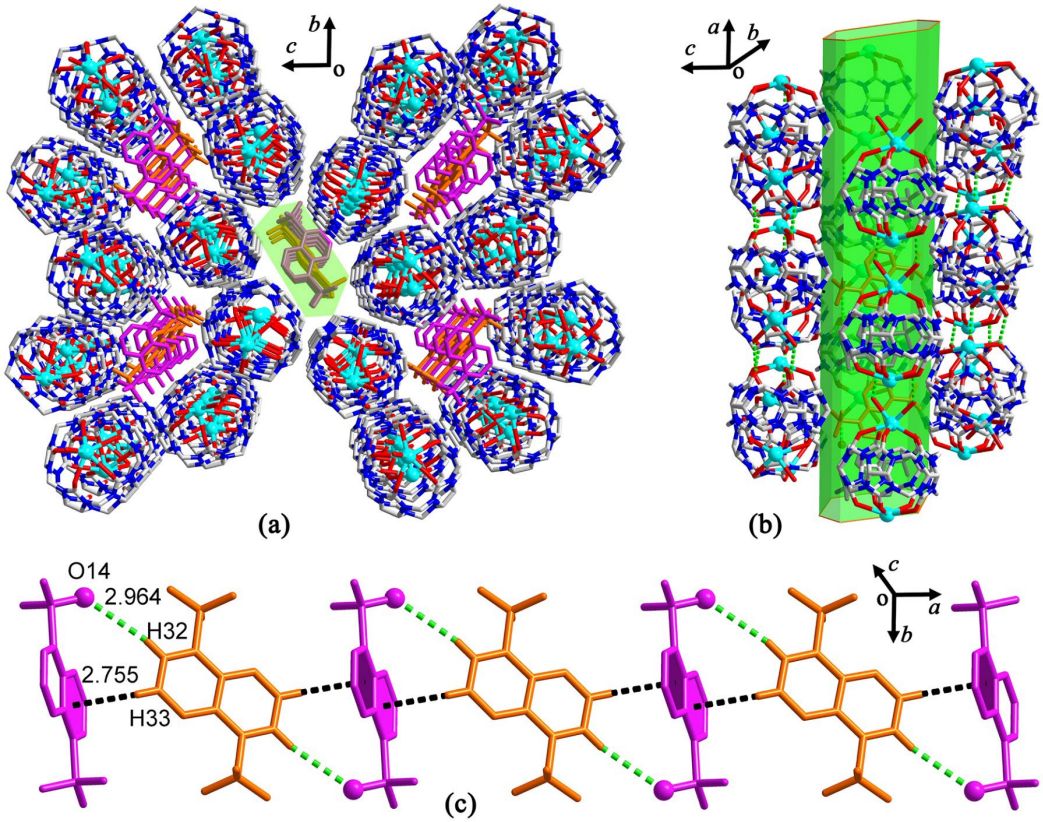

Figure 10. (a) The coordination environment of K^+ in **4** with the ellipsoids drawn at the 50% probability level. The hydrogen atoms are omitted for clarity; (b) The 1D supramolecular Q[5]-K^+ chain; (c) The final 3D supramolecular architecture of assembly **4**; (d) The 1D hexagonal channel in **4**; (e) The supramolecular 1,5-NAS^{2-} chain built through the noncovalent interactions between sulfonate ligands.

PXRD measurements were conducted to check the bulk-phase purity of the as-synthesized assemblies **1**-**6**. As shown in Figure S2, the experimental PXRD patterns of the obtained assemblies all closely matched the simulated patterns obtained from the SC-XRD data, indicating the phase purity of the obtained assemblies.

Adsorption of Dye by compound 1

As shown in **Figure 11**, five dyes with different sizes and charges, namely negatively charge IC, MO and positively charged CV, MLB and AR, were selected to evaluate the

capability of assembly **1** in the adsorption of dyes. Before the adsorption experiments, samples of **1** were first fully ground and then immersed in solutions of the dyes. Upon the addition of the powder samples of **1** into the solutions containing the different dyes, it was observed that the colors of the aqueous solutions of the anionic dyes, AR, CV and MLB all rapidly lightened and became almost colorless within 180 min, while the colors of the IC and MO aqueous solutions mostly remained unchanged, which was also demonstrated by the UV-vis spectra (**Fig. 12**). As shown in Figure 11, the absorption bands of AR around 527 nm, CV around 575 nm and MLB around 664 nm experienced a distinct decrease, while the removal efficiency of AR, CV and MLB reached 92, 95 and 85 % respectively. Only slight decreases could be observed for the absorption bands of IC and MO. Such phenomenon clearly indicated that assembly **1** could absorb anionic dyes AR, CV and MLB form aqueous media. Furthermore, in order to study the adsorption selectivity for dyes, the powder samples of assembly **1** were poured into mixed solutions containing AR/IC, AR/MO, CV/IC, CV/MO, MLB/IC and MLB/MO separately. As shown in **Fig. 13**, it was found that the colors of the mixed solutions all became similar to that of the solutions containing anionic dyes. Meanwhile, the UV-vis spectra also revealed that the characteristic absorption bands of the cationic dyes almost vanished while those of the anionic dyes scarcely changed, which demonstrated the adsorption selectivity towards cationic dyes of assembly **1**.

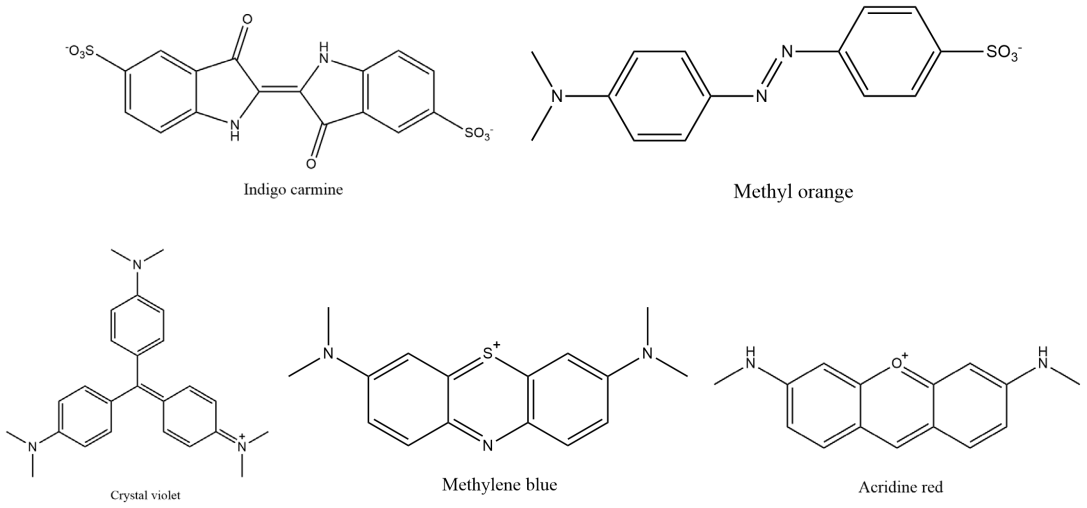

Figure 11. The structure of the dyes used in this work.

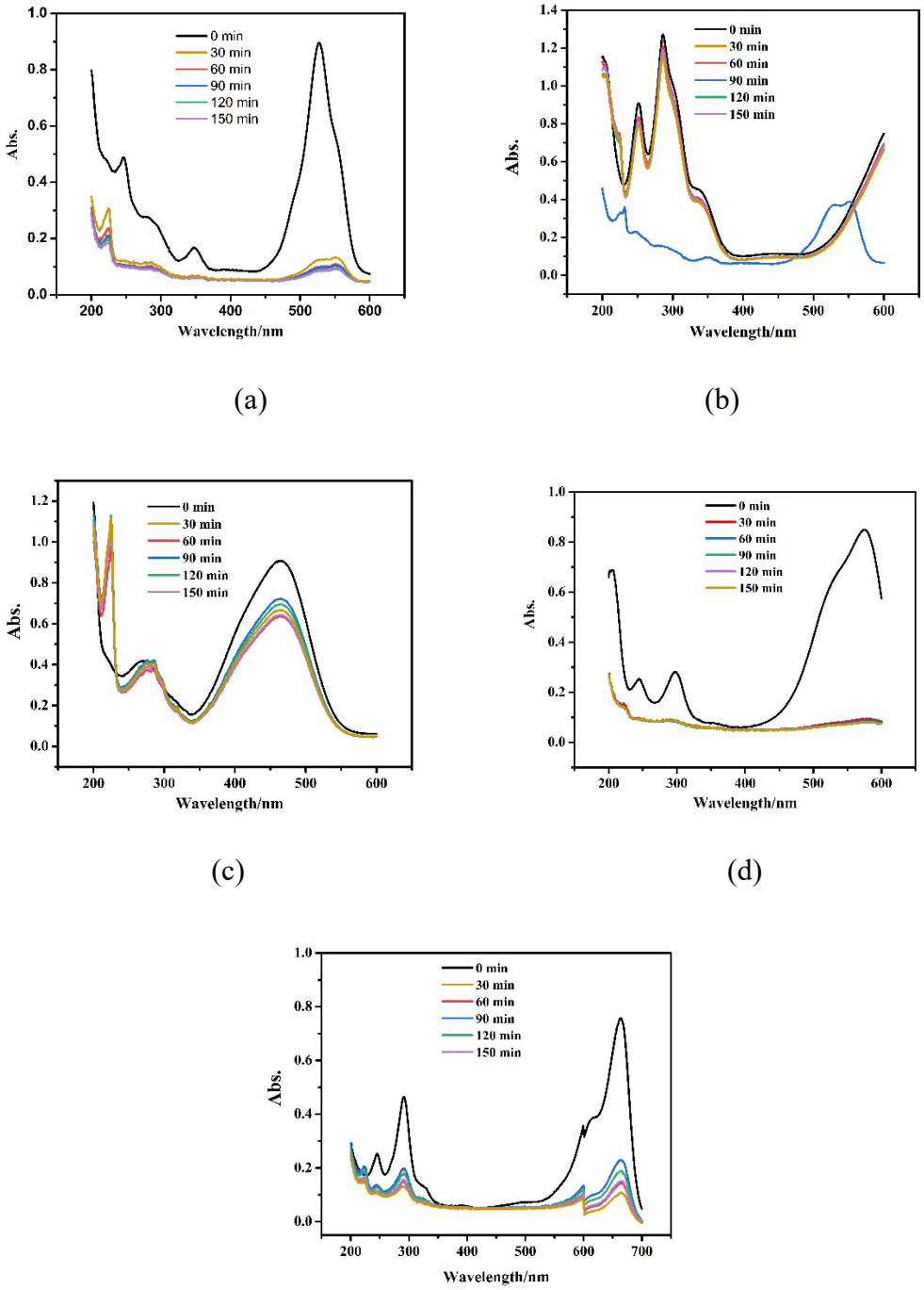

Figure 12. UV-vis spectra of the solutions containing AR (a), IC (b), MO (c), CV (d) and MLB (e) after the addition of powder samples of assembly **1**; (f) Photograph shows the change in the color of the solutions containing different dyes upon the addition of assembly **1**.

Considering that the adsorption-based solid materials exhibit different colors after

immersion in the different dye solutions, they may be applied as solid fluorescence materials. Therefore, the fluorescence properties of dye-loaded **1** were investigated in the solid state. It is interesting that the interactions of the different dyes with assembly **1** generated different fluorescence phenomena. As illustrated in **Figure 14a**, loading assembly **1** with AR, CV and MLB could separately generate a powder that appeared red, bright-purple and blue under daylight. The fluorescence spectra exhibited that AR, CV and MLB-loaded assembly induced deep-red, carmine and black-blue fluorescence emission with the maxima intensities at 630, 350 and 420 nm, respectively. Compared to the free dyes, the dye-loaded solid materials not only exhibited significant changes in color but also strengthened the emission intensities. Such results suggest that the dye-loaded Q[5]-H_2NDS assembly could form functional fluorescence materials.

Conclusions

In summary, we have demonstrated the structure-directing role of H_2NDS in the construction of Q[5]-based supramolecular assemblies. By comparing the assemblies with and without H_2NDS, it can be concluded that the outer-surface interactions of Q[5] with H_2NDS have an important effect on the structure of the obtained supramolecular assemblies. Then, H_2NDS was introduced as the structure-directing agent into the Q[5]-M_{alkali}^+ system and four novel supramolecular assemblies with similar structure were synthesized. The main difference among these four assemblies was the coordination mode adopted by the central metal ions. Furthermore, the Q[5]-H_2NDS assembly **2** without any metal ions was found to be capable of absorbing anionic dyes AR, CV and MLB from aqueous media and the dye-loaded samples could function as solid fluorescence materials.

Supplementary materials

CCDC 2219387-2219392 contain the supplementary crystallographic data for this paper. The data can be obtained free of charge via www.ccdc.cam.ac.uk/data_request/cif (or from The Cambridge Crystallographic Data Centre, 12, Union Road, Cambridge CB2 1EZ, UK; fax: +44 1223 336 033; e-mail: deposit@ccdc.cam.ac.uk).

Acknowledgments

We acknowledge the support of National Natural Science Foundation of China (No. 21601090), and the Natural Science Foundation of Jiangsu Province (Grant No. BK20160943). Dr. K. Chen thanks Major Project of Basic Science (Natural Science) Research in Higher Education Institutions of Jiangsu Province (Grant No. 22KJA150002). This work was supported by Zhuhai Talent Recruitment Grant for the Artificial Intelligence-aided Membrane Protein Drug Discovery Innovation Team (Grant No. 2120004000201). CR thanks the University of Hull for support.

Reference

[1] B. O. Okesola, D. K. Smith, Applying low-molecular weight supramolecular gelators in an environmental setting–self-assembled gels as smart materials for pollutant removal, *Chem. Soc. Rev.*, **2016**, *45*, 4226-4251.

[2] R. Zhao, Y. Wang, X. Li, B. L. Sun, C. Wang, Synthesis of β-cyclodextrin-based electrospun nanofiber membranes for highly efficient adsorption and separation of methylene blue, *ACS Appl. Mater. Interfaces*, **2015**, 7, 26649-26657.

[3] J. Qiu, Y. Feng, X. Zhang, M. Jia, J. Yao, A new route to the shape-controlled synthesis of nano-sized γ-alumina and Ag/γ-alumina for selective catalytic reduction of NO in the presence of propene, *J. Colloid interface Sci.*, **2017**, *499*, 151-158.

[4] K. Mohanty, J. T. Naidu, B. Meikap, M. Biswas, Removal of crystal violet from wastewater by activated carbons prepared from rice husk, *Ind. Eng. Chem. Res.*, **2006**, *45*, 5165-5171.

[5] X. Li, L. Xie, X. Yang, X. Nie, Adsorption behavior and mechanism of β-cyclodextrin–styrene-based polymer for cationic dyes, *RSC Adv.*, **2018**, *8*. 40321-40329.

[6] X. H. Wang, C. L. Jiang, B. X. Hou, Y. Y. Wang, C. Hao, J. B. Wu, Carbon composite lignin-based adsorbents for the adsorption of dyes, *Chemosphere*, **2018**, *206*, 587-596.

[7] M. A. M. Salleh, D. K. Mahmoud, W. A. W. A. Karim, A. Idris, Cationic and anionic

dye adsorption by agricultural solid wastes: a comprehensive review, *Desalination*, **2011**, *280*, 1-13.

[8] L. Abramian, H. EI-Rassy, Adsorption kinetics and thermodynamics of azo-dye Orange II onto highly porous titania aerogel, *Chem. Eng. J.*, **2009**, *150*, 403-410.

[9] Y. Shang, Y. P. Cui, R. X. Shi, P. Yang, J. P. Wang, Y. Z. Wang, Regenerated WO2. 72 nanowires with superb fast and selective adsorption for cationic dye: Kinetics, isotherm, thermodynamics, mechanism, *J. Hazard. Mater.*, **2019**, *379*, 120834.

[10] Y. Wang, Y. Xie, Y. Zhang, S. Tang, C, Guo, J. Wu, R. Lau, Anionic and cationic dyes adsorption on porous poly-melamine-formaldehyde polymer, *Chem. Eng. Res. Des.*, **2016**, *114*, 258-267.

[11] E. Alver, A. U. Metin, Anionic dye removal from aqueous solutions using modified zeolite: Adsorption kinetics and isotherm studies, *Chem. Eng. J.*, **2012**, *200*, 59-67.

[12] N. Abidi, E. Errais, J. Duplay, A. Berez, A. Jrad, G. Schaefer, M. Ghazi, K. Semhi, M. Trabelsi-Ayadi, Treatment of dye-containing effluent by natural clay, *J. Cleaner Prod.*, **2014**, *86*, 432-440.

[13] P. C. Su, X. Zhang, Z. H. Xu, G. L. Zhang, C. Shen, Q. Meng, Amino-functionalized hypercrosslinked polymers for highly selective anionic dye removal and CO2/N2 separation, *New. J. Chem.*, **2019**, *43*, 17267-172274.

[14] L. M. Zhang, Y. J. Zhou, Y. Wang, Novel hydrogel composite for the removal of water-soluble cationic dye, *J. Chem. Technol. Biotechnol.*, **2006**, *81*, 799-804.

[15] N. Kataria, V. K. Garg, Application of EDTA modified Fe3O4/sawdust carbon nanocomposites to ameliorate methylene blue and brilliant green dye laden water, *Environ. Res.*, **2019**, *172*, 43-54.

[16] D. N. Jiang, M. Chen, H. Wang, G. M. Zeng, D. L. Huang, M. Cheng, Y. Liu, W. J. Xue, Z. W. Wang, The application of different typological and structural MOFs-based materials for the dyes adsorption, *Coord. Chem. Rev.*, **2019**, *380*, 471-483.

[17] Y. Gao, S. Q. Deng, X. Jin, S. L. Cai, S. R. Zheng, W. G. Zhang, The construction of amorphous metal-organic cage-based solid for rapid dye adsorption and time-dependent dye separation from water, *Chem. Eng. J.*, **2018**, *357*, 129-139.

[18] Y. Li, C. X. Yang, H. L. Qian, X. Zhao, X. P. Yan, Carboxyl-functionalized covalent

organic frameworks for the adsorption and removal of triphenylmethane dyes, *ACS Appl. Nano Mater.*, **2019**, *2*, 7290-7298.

[19] Y. J. Zhou, K. C. Jie, R. Zhao, F. H. Huang, Supramolecular-Macrocycle-Based Crystalline Organic Materials, *Adv. Mater.*, **2020**, *32*, 1904824.

[20] J. R. Wu, Y. W. Yang, Separation of bromoalkanes isomers by nonporous adaptive crystals of leaning pillar[6]arene, *Angew. Chem. Int. Ed.*, **2020**, DOI:10.1002/anie.202006999.

[21] M. C. L. Yeung, V. W. W. Yam, Luminescent cation sensors: from host–guest chemistry, supramolecular chemistry to reaction-based mechanisms, *Chem. Soc. Rev.*, **2015**, *44*, 4192-4202.

[22] W. W. Fang, Y. Zhang, J. J Wu, C. Liu, H. B. Zhu, T. Tu, Recent Advances in Supramolecular Gels and Catalysis, *Chem. Asian J.*, **2018**, *13*, 712-729.

[23] O. J. G. M. Goor, S. I. S. Hendrikse, P. Y. W. Dankers, E. W. Meijer, From supramolecular polymers to multi-component biomaterials, *Chem. Soc. Rev.*, **2017**, *46*, 6621-6637.

[24] L.W. Yan, M. Q. Lv, C. J. Su, L. H. Zheng, J. L. Li, Z. B. Ye, An efficient supramolecular adsorbent for co-adsorption of dyes and metal ions from wastewater and its application in self-healing materials, *Soft Matter*, **2017**, *12*, 8772-8780.

[25] X. T. Qin, G. N. Zhang, Y. F. Gao, H. T. Liu, C. F. Du, Z. L. Liu, Metallo-supramolecular grid-type architectures for highly and selectively efficient adsorption of dyes in water, *RSC Adv.*, **2015**, *5*, 43334-43337.

[26] J. T. Ma, Y. Zhang, B. F. Zhao, Q. Jia, Supramolecular adsorbents in extraction and separation techniques - A review, *Anal. Chim. Acta*, **2020**, *1122*, 97-113.

[27] J. Lagona, P. Mukhopadhyay, S. Chakrabarti, L. Isaacs, The Cucurbit[n]uril Family, *Angew. Chem. Int. Ed.*, **2005**, *44*, 4844-4870.

[28] J. W. Lee, S. Samal, N. Selvapalam, H. J. Kim, K. Kim, The Cucurbit[n]uril Family, *Acc. Chem. Res.*, **2003**, *36*, 621-630.

[29] E. Masson, X. X. Ling, R. Joseph, L. Kueremeh-Mensah, X. Y. Lu, Cucurbituril chemistry: a tale of supramolecular success, *RSC Adv.*, **2012**, *2*, 1213-1247.

[30] S. J. Barrow, S. Kasera, M. J. Rowland, J. del Barrio, O. A. Scherman,

Cucurbituril-based molecular recognition, *Chem. Rev.*, **2015**, *115*, 12320-12406.

[31] X. L. Ni, X. Xiao, H. Cong, L. L. Liang, K. Cheng, X. J. Cheng, N. N. Ji, Q. J. Zhu, S. F. Xue, Z. Tao, Cucurbit[n]uril-based coordination chemistry: from simple coordination complexes to novel poly-dimensional coordination polymers, *Chem. Soc. Rev.*, **2013**, *42*, 9480-9508.

[32] J. Lu, J. X. Lin, M. N. Cao, R. Cao, Cucurbituril: A promising organic building block for the design of coordination compounds and beyond, *Coord. Chem. Rev*., 2013, 257, 1334-1356.

[33] W. A. Freeman, W. L. Mock, N. Y. Shih, Cucurbituril, *J. Am. Chem. Soc.*, **1981**, *103*, 7367-7368.

[34] F. Zhang, T. Yajima, Y. Z. Li, G. Z. Xu, H. L. Chen, Q. T. Liu, O. Yamauchi, Iodine-Assisted Assembly of Helical Coordination Polymers of Cucurbituril and Asymmetric Copper(II) Complexes, *Angew. Chem., Int. Ed.*, **2005**, *44*, 3402-3407.

[35] X. L. Ni, X. Xiao, H. Cong, Q. J. Zhu, S. F. Xue, Z. Tao, Self-Assemblies Based on the "Outer-Surface Interactions" of Cucurbit[n]urils: New Opportunities for Supramolecular Architectures and Materials, *Acc. Chem. Res.*, **2014**, *47*, 1386-1395.

[36] Y. Q. Yao, Y. J. Zhang, Y. Q. Zhang, Z. Tao, X. L. Ni, G. Wei, Multiple Efficient Fluorescence Emission from Cucurbit[10]uril-[Cd4Cl16]8–-Based Pillared Diamond Porous Supramolecular Frameworks, *ACS Appl. Mater. Interfaces*, **2017**, *9*, 40760-40765.

[37] R. H. Gao, Y. Fan, B. Xiao, P. Chen, J. X. Zhang, Q. D. Zhou, S. F. Xue, Q. J. Zhu, Zhu Tao, Direct syntheses of cucurbit[7]uril-anchored polyacrylic acid microspheres and adsorption of basic dyes by the derivative, *RSC Adv.*, **2015**, *5*, 65775-65779.

[38] X. Tian, L. X. Chen, Y. Q. Yao, K. Chen, M. D. Chen, X. Zeng, Z. Tao, 4-Sulfocalix[4]arene/Cucurbit[7]uril-Based Supramolecular Assemblies through the Outer Surface Interactions of Cucurbit[n]uril, *ACS Omega*, 2018, 3, 6665-6672.

[39] X. X. Wang, F. Y. Tian, K. Chen, Y. Q. Zhang, Z. Tao, Q. J. Zhu, Hexamethylcucurbit[3, 3]uril-Based Porous Supramolecular Assemblies and Their Adsorption Properties, *ACS Omega*, 2018, 3, 9827-9833.

[40] Z. Li, L. Li, D. L. Hu, C. Gao, J. Y. Xiong, H. Y. Jiang, W. Li, Efficient removal of

heavy metal ions and organic dyes with cucurbit [8] uril-functionalized chitosan, *J. Colloid Interface Sci*., 2019, 539, 400-413.

[41] Y. Luan, H. F. Liu, Z. Qiao, B. H. Koo, J. Shin, Y. O. Jang, J. S. Noh, Y. Shin, Efficient removal of heavy metal ions and organic dyes with cucurbit[8]uril-functionalized chitosan, *Sci. Rep.*, **2020**, *10*, 443.

[42] A. Day, A. P. Arnold, R. J. Blanch and B. Snushal, Controlling factors in the synthesis of cucurbituril and its homologues, *J. Org. Chem.*, **2001**, *66*, 8094–8100.

[43] SAINT, Program for Data Extraction and Reduction, Bruker AXS, Inc., Madison, WI, 2001.

[44] G. M. Sheldrick, SADABS, Program for Empirical Adsorption Correction of Area Detector Data, University of Gottingen, Gottingen, Germany, 2003.

[45] (a) G. M. Sheldrick, SHELXS-2014, Program for the Crystal Structure Solution, University of Gottingen, Gottingen, Germany, 2014; (b) G. M. Sheldrick, SHELXL-2014, Program for the Crystal Structure Solution, University of Gottingen, Gottingen, Germany, 2014.